Dynamics of paramagnetic microrod in a viscous medium under rotating magnetic fields

Author: Ferran Jiménez Cuélliga.
Facultat de Física, Universitat de Barcelona, Diagonal 645, 08028 Barcelona, Spain.

Advisor: Carles Calero Borrallo
(Dated: June 22, 2021)

Abstract: In this work we study the dynamics of magnetic rods in viscous media under rotating magnetic fields. We analyze the rotation dynamics of a paramagnetic and a ferromagnetic rods under rotating fields with circular and elliptical polarization in the bulk of a viscous liquid using the slim-body approximation. We also simulate the same setup using molecular dynamics simulations and validate the results for the paramagnetic rod in the bulk. Since we recover the theoretical behaviour we simulate the dynamics of the paramagnetic rod in presence of a wall. We then confirm that under elliptically polarized rotating fields the paramagnetic microrod can act as a toggleable microswimmer.

I. INTRODUCTION

The study of the dynamics of micro and nanometrical devices in viscous media is important from a fundamental level and for the potential applications that it can have in a range of fields. For example, they can be used to transport medicine in the human body, manufacture magnetic devices [1], biosensors [2] among other applications.

Due to the typical sizes and velocities involved, the dynamics of these objects in viscous liquids occurs at very low Reynolds numbers. In this regime, the inertial terms in the Navier-Stokes equation for hydrodynamics are irrelevant and the equation becomes time reversible. As a consequence, any swimming strategy based on backward and forward displacements, will not induce net propulsion [3]. To overcome this difficulty it is known that in low Reynolds regime, the rotation of a body in proximity of a surface can translate into net translation due to the hydrodynamic interaction with the boundary.[4]

Magnetic microparticles are good candidates to be transported on surfaces, since they can be externally controlled using magnetic fields. The dynamics of magnetic particles strongly depend on their magnetic response. A ferromagnetic rod rotates at any frequency in a rotating magnetic field [4] whereas a paramagnetic rod will stop rotating after a certain magnetic frequency when submerged in bulk [1].

The aim of this work is to study through numerical calculations the propulsion of a paramagnetic microrod on top of a bounding surface under the actuation of rotating magnetic fields. First, I analyze the rotation dynamics of a paramagnetic and a ferromagnetic rods under rotating fields with circular and elliptical polarization in the bulk of a viscous liquid. I reproduced the results of Ref. [1] for the dynamics of a paramagnetic rod under rotating fields. I confirmed that for a certain frequency the microrod stops rotating and begins oscillating around a given axis. Next, I used the same treatment to study the dynamics of the ferromagnetic case. Although this theoretical treatment is simple, its extension to account for a bounding plane is not possible. To perform such analysis we employ numerical simulations of a model of a rod in a viscous fluid. I modified an existing simulation code to describe the interaction of the paramagnetic rod with an external field. I tested the code against the numerical treatment based on [1], with good agreement. Finally, we included a bounding plane in the simulation code and performed simulations under different magnetic actuations. We demonstrate that under elliptically polarized actuations net movement is achieved while below a certain critical frequency.

II. THEORETICAL MODEL

Let us consider a magnetic rod composed of N spherical particles under a rotating magnetic field. The dynamics under low Reynolds number conditions can be obtained as to a torque balance equation.

To describe the dynamics of the rod we first reproduce the theoretical description of Helgesen and co-workers[1]. The dynamics is governed by the balance of two main torques which act on the rod. First, the external magnetic field exerts a torque on the rod. Its form depends on the magnetic response of the rod, either paramagnetic or ferromagnetic. Being at very low Reynolds number, this torque is compensated by the hydrodynamic torque exerted by the viscous fluid, which opposes the rotations of the bar.

A. Hydrodynamic drag

To describe the hydrodynamic drag of the fluid with the elongated bar, we use the slim object approximation. The slim object approximation imagines the N-colloid rod as a continuous rod with a characteristic length L, much larger that its width d.

The fluid torque for the slim object approximation [5]

is given by:

$$M_L = \frac{-4\pi\eta L^3}{12\gamma}\frac{d\phi_r}{dt} \tag{1}$$

where η is the liquid's viscosity, ϕ_r is the rod's angle in respect of its initial position, γ is a slimness ratio. When we take into account that the length of the bar is $L = Nd$, as the rod will be formed by N balls of diameter d, and that $\gamma = ln(\frac{L}{d})$

$$M_L = \frac{-4\pi\eta L^3}{12\ln(\frac{L}{d})}\frac{d\phi_r}{dt} = \frac{-4\pi\eta(Nd)^3}{12\ln(N)}\frac{d\phi_r}{dt} \tag{2}$$

B. Paramagnetic Rod

The magnetic dipole-dipole interaction energy is given by:

$$H = -\frac{\mu_0}{4\pi|\mathbf{r}|^3}\left(3(\mathbf{m}_1\cdot\hat{\mathbf{r}})(\mathbf{m}_2\cdot\hat{\mathbf{r}}) - \mathbf{m}_1\cdot\mathbf{m}_2\right) \tag{3}$$

where $\mathbf{m}_1$ and $\mathbf{m}_2$ are the dipoles' magnetic momentum. The external magnetic field is $\mathbf{B} = B_x\cos(\omega_H t)\mathbf{e}_x + Bz\sin(\omega_H t)\mathbf{e}_z$. The magnetic moment of the paramagnetic particles is then given by $\mathbf{m} = \frac{4\pi(\frac{d}{2})^3}{3\mu_0}\chi_{eff} * \mathbf{B}$ where χ_{eff} is the effective volume susceptibility of the paramagnetic particles. Considering that the the N-spheres' momenta are all parallel to each other and form an angle the magnetic dipolar energy is:

$$H = \sum_{i=1}^{N}\sum_{i<j}^{N} -\frac{\mu_0 m^2}{4\pi|\mathbf{r_{ij}}|^3}(3cos(\theta) - 1) \tag{4}$$

where $r_{ij} = d|j-i|$ and θ is the angle between the microrod and the external field. Arriving to the expression:

$$H = -\frac{\mu_0 m^2}{4\pi|d|^3}(3\cos(\theta) - 1)\sum_{i=1}^{N}\sum_{i<j}^{N}\frac{1}{|j-i|^3} \tag{5}$$

We approximate the sum over j in Eq.(5) by its value for $N \to \infty$, which is given by $\sum_{i=1}^{\infty}\sum_{i<j}^{\infty}\frac{1}{|j-i|^3} = N\zeta(s=3)$, where $\zeta(s=3)$ is Riemann's zeta function for s=3. The value of this function for s=3 is $\sum_{i=1}^{\infty}\frac{1}{i^3} = \zeta(s=3) = 1,20205..$, which is Apéry's constant.

Finally, the total magnetic energy is then approximated to:

$$H = -\frac{1.202N\mu_0 m^2}{4\pi|d|^3}(3\cos(\theta) - 1) \tag{6}$$

Consequently the magnetic torque acting on the bar due to the magnetic interaction is $M_H = -\frac{dH}{d\theta}$:

$$M_H = CA(t)sin(2\theta) \tag{7}$$

where $C = \frac{1.202N\pi\chi_{eff}^2 d^3 B_x^2}{48\mu_0}$, $A(t) = [\cos^2(\omega_H t) + r^2\sin^2(\omega_H t)]$, which comes from the external magnetic field.$\theta = tan^{-1}(rtan(\omega_H t) - \phi_r)$ and $r = \frac{H_z}{H_x}$ determines the degree of ellipticity of the external actuation.

Balancing the torques given by Eq.(2) and Eq.(7) results in the following differential equation:

$$\frac{d\phi_r}{dt} = -\frac{1.202\chi_{eff}^2\ln(N)B_x^2}{16N^2\eta\mu_0}A(t)sin(2\theta) \tag{8}$$

Defining $\omega_c = -\frac{1.202\chi_{eff}^2\ln(N)B_x^2}{16N^2\eta\mu_0}$ reduces Eq.(8) to the problem solved in [1]. ω_c is a characteristic frequency which defines the timescale of the problem.

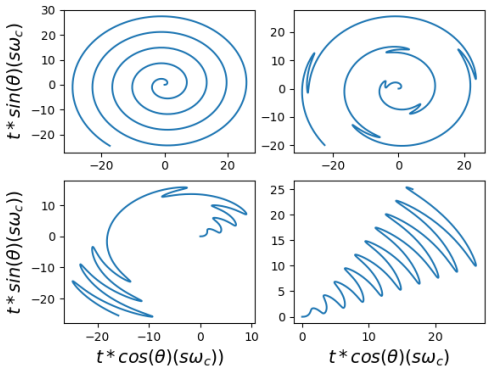

FIG. 1: Polar representation of the rod's angle in four different regimes. a)Synchronous rotation for r=1 when $\omega_h = \omega_c$ b) Asynchronous oscillations for $\omega_h > \omega_c$ c)Asynchronous oscillations for $\omega_{c2} > \omega_h > \omega_{c1}$ for r=0.7 d)Oscillations around a set axis for r=0.7 and $\omega_h > \omega_{c2}$

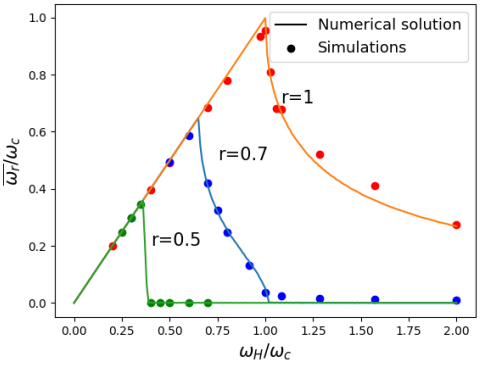

FIG. 2: Dependence of the mean angular frequency of the paramagnetic rod on the magnetic field frequency in units of the critical frequency for r=1. The numerical solutions are in units of ω_{cth} and the simulation results in units of ω_{csim}. Three different behaviours are represented for three different values of r.

I solved Eq.(8) numerically using a Runge-Kutta 4 algorithm for different values of ω_H and r. The results are

represented in Fig. 1. We can see different behaviours. For r=1 and $\omega_H < \omega_c$, the rod rotates at the same rate as the field as shown in Fig. 1a. For $\omega_H > \omega_c$ the rod has periods of forward and backward motion, see Fig. 1b. The average angular velocity of the rod $\overline{\omega_r}$ will tend to 0 when $\omega_H \to \infty$.

For r<1, there are three regimes. There is a first transition frequency $\omega_{c1}$from which the rod will stop rotating at the same rate as the field and start presenting forward and backward rotations (see Fig. 1c). There is also a second transition after a second critical frequency ω_{c2} in which the rod oscillates about a fixed axis, and the average angular velocity of the rod $\overline{\omega_r} = 0$ see Fig.1d.

C. Ferromagnetic Rod

For a rigid rod composed of N ferromagnetic particles with identical magnetic moment m directed along the axis of the rod, the magnetic torque with the external field is given by

$$\tau = \sum_{i=1}^{N} \mathbf{m} \times \mathbf{B} = N|m||B|sin(\theta) \tag{9}$$

Applying the torque balance between hydrodynamic drag torque Eq.(2) and the magnetic torque Eq.(9) , a similar differential equation is obtained:

$$\frac{d\phi_r}{dt} = -\frac{\mathcal{M}B_x}{2\eta N^2}\sqrt{A(t)}sin(\theta) \tag{10}$$

with the same A(t) and θ of the paramagnetic case and where we used $m = \frac{4\pi}{3}(\frac{d}{2})^3\mathcal{M}$, being $\mathcal{M}$, the magnetization of the ferromagnet. We can also define a characteristic frequency $\omega_c^f = \frac{\mathcal{M}B_x}{2\eta N^2}$

The numerical solution of Eq.(10) is represented in Fig. 3 for different values of the critical frequency ω_c^f. As shown in the figure, the critical behaviour in the ferromagnetic case shows that no matter the value of r, the mean angular velocity of the rod will only approach zero asymptotically, which is in accordance to the experimental results. [2]

D. Comparison

A few observations can be made. Neither for the paramagnetic nor the ferromagnetic rods does the critical frequency ω_c or ω_c^f depend on the size of the rod, only on the number of spheres it is made of. That is under the condition that all the spheres are in contact with the contiguous spheres, this is due to both the magnetic and fluid torques scaling with the volume of the spheres.

The value of ω_c scales with the squared of the magnetic field for the paramagnetic rod, while the critical frequency for the ferromagnetic scales with the product of $\mathcal{M}$ and the magnetic field.

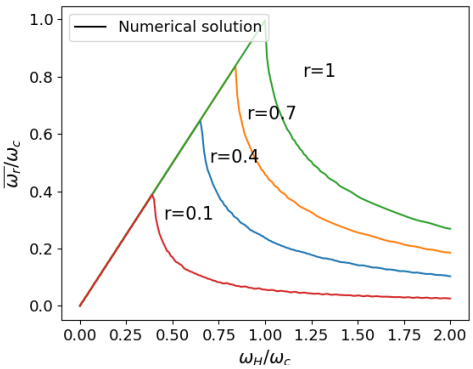

FIG. 3: Mean angular frequency of the ferromagnetic rod as a function of the magnetic field frequency in units of the numerical critical frequency for r=1

The differential equations governing the dynamics of the ferromagnetic and paramagnetic rods, Eqs. (10) and (8), present two main differences. While for the paramagnetic rod the differential equation depends on A(t) and sin(2θ), for the ferromagnetic case it depends on $\sqrt{A(t)}$ and sin(θ)

III. SIMULATION MODEL

We also solved the dynamics of the paramagnetic rod using dynamic simulations of a point-particle based model. Instead of considering the rod a continuous object we'll consider 10 equally spaced paramagnetic point particles which interact magnetically among each other and with the fluid they inhabit.

The rod keeps a fixed distance using a constraint SHAKE algorithm [6]. The hydrodynamics are implemented using Oseen's tensor which is Green's solution to the Stokes equation to simulate fluid flow with no boundary conditions. Oseen's tensor connects the force exercised on a point $\mathbf{r}_i$ to the resulting fluid flow at $\mathbf{r}$ [10]. The flow generated by a point particle is given by:

$$\mathbf{u}(\mathbf{r}) = \frac{1}{8\pi\eta}(\frac{1}{r}\hat{\mathbf{I}} + \frac{(\mathbf{r}-\mathbf{r}_i)(\mathbf{r}-\mathbf{r}_i)}{|\mathbf{r}-\mathbf{r}_i|^3}) * \mathbf{f}(\mathbf{r}_i) \tag{11}$$

where $\hat{\mathbf{I}}$ is the identity matrix.

The equations of motion for the particles that form the paramagnetic rod are

$$m\frac{d\mathbf{v_i}}{dt} = \mathbf{F_i} - \gamma(\mathbf{v_i} - \mathbf{u}(\mathbf{r_i})) \tag{12}$$

where m is the mass of the particle, $\mathbf{v_i}$ its velocity, $\mathbf{F_i}$ is the external force on particle i, and $\gamma_0 = 3\pi\eta d$ is the drag coefficient. These equations are numerically solved using a modified Verlet algorithm, which solves Newton's equation in discrete time steps. This algorithm computes the position and velocity of the next step using:

$$r_i(t+\Delta t) = r_i(t) + v_i \Delta t + \frac{f_i(t)}{2m_i}\Delta t^2 \tag{13}$$

$$v_i(t+\Delta t) = \frac{2m - \gamma_0 \Delta t}{2m + \gamma_0 \Delta t} v_i(t) + \frac{f_i(t) + f_i(t+\Delta t)}{2m_i + \gamma_0 \Delta t}\Delta t \tag{14}$$

A. Dynamics of the paramagnetic rod

We simulated the behaviour for various values of r, and with a magnetic field of 250mT. The dynamics of the rod obtained from our simulations are represented in Fig. 2. As shown in the figure, the behavior observed follows the same trends obtained from the numerical solution of Eq.(8) for different values of r. The theoretical estimate for the critical frequency provides a value of wc = 2984Hz. We can also determine the critical frequency from simulations of the model at different frequencies, resulting in $\omega_c^{sim} \approx 700Hz$. This discrepancy might appear because we supposed N to be very large when applying the slim object approximation. We can check that for $\omega_c = 700$Hz the Reynold's number $Re = \frac{uL\rho}{\eta} \approx 10^{-3}$ and thus we are still in a low Reynolds regime at this range of frequencies. We have identified the critical frequency for different values of the magnetic field performing different sets of simulations. As shown in Fig. 4, we obtain a clear linear dependence of the critical frequency on the magnitude of the field, as expected for paramagnetic particles. With a lineal regression we can see $\omega_{csim} = 10485B_x^2 + 6.8717$

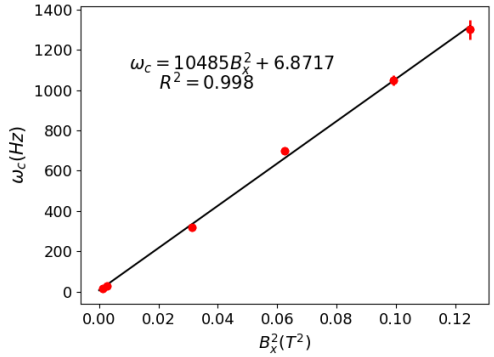

FIG. 4: Dependency of the critical frequency on B_x^2

B. Simulations in presence of a wall

Having checked that simulations reproduce well the behavior expected in bulk, we have finally included in our simulations the presence of a wall. We expect that its presence can rectify the rotation of the rod into net propulsion

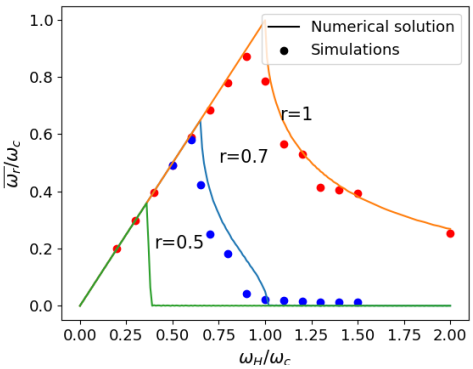

FIG. 5: Mean angular frequency of a rod as a function of the field's frequency in units of the critical frequency for r=1. The numerical solution is in absence of a wall while the simulations results are in presence of a wall and in the bulk's critical frequency units

The particles forming the rod interact with the wall at z = 0 through a repulsive short range interaction given by

$$U(z) = 4\left[\left(\frac{d}{z}\right)^{12} - \left(\frac{d}{z}\right)^{6}\right], \qquad z < 2^{1/6}d \tag{15}$$

and U(z) = 0 for $z > 2^{1/6}d$. In addition, the hydrodynamic flow is modified by the presence of the wall. Assuming no-slip boundary conditions at the wall, the hydrodynamic flow due to a point particle is given by the Blake tensor instead of the Oseen tensor.[7]

We have performed simulations including the presence of the wall. The results for the frequency of rotation of the rod are represented in Fig.5 as a function of the field's frequency. As shown in the figure, we observe a similar behavior as the one obtained in bulk, although some minor differences in the average angular velocity appear. This might be due to hydrodynamic effects of the walls and because the microrod may momentarily come to a halt when colliding with the wall.

C. Movement below critical frequency and elliptical field

In Fig. 6 we represent the position of the geometric center of the paramagnetic microrod in under an elliptically polarized rotating field for different frequencies. For $\omega_H < \omega_{c1}$, we find that the mean value of x displaces $0.175\mu m$ after three rotations of the magnetic field, as represented in Fig. 6. As shown in Fig. 5, at this frequency the rod rotates with the magnetic field, inducing its propulsion due to the presence of the wall. For $\omega_H > \omega_{c2}$ however, when the rod is oscillating around a

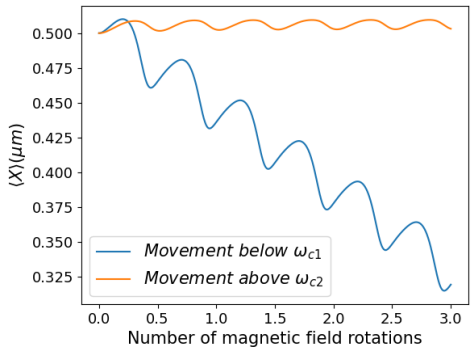

FIG. 6: Mean position of the rod throughout three full rotations of the magnetic field. Comparison between the movement of the rod when $\omega_H < \omega_{c1}$ and $\omega_H > \omega_{c2}$

set axis, there is no net displacement (see Fig. 6).We conclude that a paramagnetic rod is a toggleable microswimmer in a low Reynolds regime when applying a elliptically rotating magnetic field: while $\omega_H < \omega_{c2}$ the rod moves but when $\omega_H < \omega_{c2}$ it does not.

IV. CONCLUSIONS

We solved the dynamics of magnetic microrods immersed in a viscous fluid under the actuation of rotating magnetic fields.

First, we obtain the differential equations for the angular dynamics of paramagnetic and ferromagnetic rods using the slim body approximation. We find that the paramagnetic rod rotates with the external field under a critical frequency, from which the rod has periods of forward and backward motion. When elliptically polarized, it will stop rotating after a second critical frequency. In contrast, the ferromagnetic rod always rotates with the field.

Next, we solve the dynamics of a paramagnetic rod using molecular dynamics simulations of a model consisting of 10 equally spaced particles rigidly bonded. The results agree with the theoretical model.

Once the simulation model is tested, we include the presence of a wall to study its effects on the rotation and propulsion of the paramagnetic rod. We find that the rotational dynamics are very similar to that in the bulk. Under elliptically polarized rotating fields, the rod propels for field frequencies below a critical value ω_{c2}, but does not move for field frequencies $\omega_H > \omega_{c2}$.

Acknowledgments

I would like to express my gratitude towards my advisor Dr. Carles Calero for his support, help and guidance during all the process. I would like to thank my parents and family for their unconditional love and for always believing in me. And my friends for their patience and for always being there.

[1] Helgesen, Geir, Piotr Pieranski, and Arne T. Skjeltorp."Nonlinear phenomena in systems of magnetic holes." Physical review letters **64**.**12**: 1425. (1990)

[2] Janssen, X. J. A., et al. "Controlled torque on superparamagnetic beads for functional biosensors." Biosensors and Bioelectronics **24**.**7**: 1937-1941. (2009)

[3] Purcell, Edward M. "Life at low Reynolds number." American journal of physics **45**.**1**: 3-11. (1977)

[4] Martinez-Pedrero, Fernando, et al. "Colloidal microworms propelling via a cooperative hydrodynamic conveyor belt." Physical review letters **115**.**13**: 138301. (2015)

[5] Gutman, Emiliya, and Yizhar Or. "Optimizing an undulating magnetic microswimmer for cargo towing." Physical Review E **93**.**6**: 063105. (2016)

[6] Bailey, A. G., et al. "Accurate simulation dynamics of microscopic filaments using "caterpillar" Oseen hydrodynamics." Physical Review E **80**.**4**: 046707. (2009)

[7] Blake, J. R. *A note on the image system for a Stokeslet in a no-slip boundary.* Mathematical Proceedings of the Cambridge Philosophical Society. Vol. 70. No. 2. (Cambridge University Press, 1971).

[8] Allen, M. P., and D. J. Tildesley. "Computer Simulations of liquids, 1987." London, UK (1983).

[9] García-Torres, José, et al. "Magnetically tunable bidirectional locomotion of a self-assembled nanorod-sphere propeller." Nature communications **9**.**1**: 1-7. (2018)

[10] Duprat, Camille, and Howard A. Shore, eds. *Fluid-structure interactions in low-Reynolds-number flows.* (Royal Society of Chemistry, 2015.)